Sound-evoked auditory neurophysiological signals are a window into prodromal functional differences in a preclinical model of Alzheimer's Disease

Aysegul Gungor Aydin[1,2], Pranav Manoj[3], Faiza Ramadan[4], Sarah Rajan[4], Elias Youssef[4], Elizabeth B. Torres[6,7,8] and Kasia M. Bieszczad*[4,7,8]

Authors and Affiliations

1. **Biomedical Research Institute of New Jersey, Cedar Knolls, NJ, 07927, USA**
   Aysegul Gungor Aydin
2. **Atlantic Health System, Morristown, NJ, 07960, USA**
   Aysegul Gungor Aydin
3. **Rutgers Robert Wood Johnson Medical School, New Brunswick, NJ, 08901, USA**
   Pranav Manoj
4. **Department of Psychology—Behavioral and Systems Neuroscience, Rutgers University, Piscataway, NJ, 08854, USA**
   Elias Youssef, Sarah Rajan, Faiza Ramadan & Kasia M. Bieszczad
5. **Department of Psychology—Cognitive Psychology, Rutgers University, Piscataway, NJ, 08854, USA**
   Elizabeth B Torres
6. **Computational Biomedicine Imaging and Modelling, Rutgers University, Piscataway, Piscataway, NJ, 08854, USA**
   Elizabeth B Torres
7. **Rutgers Center for Cognitive Science (RuCCS), Rutgers University**
   Kasia M. Bieszczad and Elizabeth B Torres
8. **Department of Head & Neck Surgery and Communication Sciences, Rutgers Robert Wood Johnson Medical School, New Brunswick, NJ, 08901, USA**
   Kasia M. Bieszczad

Corresponding author

Correspondence to Dr. Kasia M. Bieszczad
327 Psychology Building, Rutgers University-New Brunswick
152 Frelinghuysen Road
Piscataway, New Jersey 08854 USA
kasia.bie@rutgers.edu

ABSTRACT

Hearing has been identified as the largest modifiable mid-life risk factor for Alzheimer's Disease (AD), despite that its link to dementia remains unclear. Here we identify a biomarker of AD risk in an auditory neural signal using the non-invasive, rapidly acquired, and clinically translatable auditory brainstem response (ABR) in normal hearing knock-in rats (Swedish familial AD risk variant to *Amyloid precursor protein*, *App*^{S}; male and female). While ABR morphology has been proposed as a biomarker for AD, we report a novel biomarker derived from multidimensional parametric feature extraction on the distribution statistics of repeated single traces of the ABR that increases its potential for clinical utility with sensitivity and specificity. We report accurate prediction of AD genetic risk in both young and aged animals: *App*^{S} rats separate clearly from humanized controls in both sex- and age-dependent manners. Notably, auditory learning in young adulthood normalized the ABR signature in *App*^{S} rats with maintained effects into older age, altogether supporting a central neural generator of auditory dysfunction related to AD risk. These preclinical findings show how ABRs could provide a very early biomarker for detection of AD risk and lay the groundwork to test the synergy of auditory and cognitive functions in human dementia.

Keywords: Auditory system, Alzheimer's Disease, biomarker, neuroplasticity, memory, auditory brainstem response (ABR)

INTRODUCTION

Hearing loss is the largest modifiable risk factor for Alzheimer's Disease (AD) and related dementias (ADRD)[1–3]. Although the significance of auditory system processes in dementia has been validated by 20+ years of research showing links between hearing loss, cognitive decline, and cortical atrophy, mechanisms to link hearing ability with dementia remain unclear[4–7]. Hypotheses that range from causal, indirect, or common cause mechanisms to link hearing ability with dementia diagnosis are now being actively investigated in multiple disciplines[8] as a timely response to emerging evidence that correcting hearing loss with hearing aids in humans does not always mitigate AD risk[9,10]. The relationship may instead involve functional integration of auditory cortical and subcortical circuitry that directly affects learning and memory processes, the first cognitive abilities affected in ADRD. For example, animals and humans that successfully learn and remember have neuroplasticity events that rapidly and stably reorganize auditory cortical circuits to amplify representation by enhancing responses to behaviorally salient sounds[11–17]. Further, the auditory cortex is massively integrated with every subcortical processing node in the auditory system[18,19] in descending chains of projections that outweigh the ascending inputs more than 3:1[20,21]. Thus, the auditory cortex is positioned to modulate its own ascending inputs from the periphery in a way that reflects the individual's unique memories of salient sounds[22–24]. While experience-based modulation is one of its primary features, the auditory system is also a high-resolution spectrotemporal processor with the brain's fastest, most temporally precise neural activity on the microsecond scale. Neurophysiological failures in reliable and consistent neural transmission will make it harder to hear—or rather, to listen—for salient sounds[23,25]. Indeed, auditory function may be particularly susceptible to functional changes in synaptic transmission evident very early in neurodegenerative disease, potentially explaining the link between *mid-life* hearing before pathology emerges and *later* dementia risk[26,27]. This creates a compelling clinical opportunity for earlier AD/ADRD diagnoses and disease monitoring via the auditory system.

A prime auditory neurophysiological candidate to act as a sensitive biomarker of AD risk is the auditory brainstem response (ABR), which can be obtained by non-invasive EEG-like recordings. This "brainstem response" is an apparent misnomer since the ABR reflects integrated function across the entire auditory system that appears as a series of waves (I, II, III, IV, V, etc.) in a typical trial-averaged response. Each sound-evoked ABR wave has a peak amplitude and latency that reflect ascending population activity from generally-agreed upon central neural generators from the auditory nerve, to subcortical and higher auditory cortical areas[23,28]. While the gross morphology of identifiable waves is similar across subjects, the detailed morphology of the ABR is unique between individuals (in humans and rodents), and incredibly stable over time. As such, we and others have used it as an auditory fingerprint with individual differences gained by a subject's unique experiential life history[29] and potential disease states[30–32]. ABR wave amplitude and latency have been suggested as markers of mild cognitive impairment (MCI) and AD[33], but their clinical impact has been limited due to a lack of sensitivity and specificity in predicting disease state or severity. Here, we apply a novel analytical method to functionally characterize ABRs by using a multi-dimensional parametric feature space obtained from single-trial data[34]. This method allows a rich neural signature to be characterized beyond qualitative ABR morphology, amplitude, latency, or threshold assessments[35]. By applying mathematical modelling

to the distributions of single trial sound-evoked response variability across hundreds of repeated sound presentations, the parameter space in which individual subjects' responses can be classified is profoundly increased, which may increase the sensitivity and specificity of an ABR biometric for disease risk. Similar analytical methods applied to single-trial ABR data from human neonates have successfully identified unique features of variability measures that can be used remarkably early in human life to correctly predict future diagnosis of neurodevelopmental disorders that are not easily recognized until the age when neurotypical children become verbal[31].

In this report, we initially present an identified ABR diagnostic tool that characterizes dysfunction in a rat model of AD that mimics early-onset (<65 years of age) human Alzheimer's Disease via a CRISPR/Cas9-mediated Familial AD (FAD) "Swedish" risk variant *knock-in* to the genomic amyloid-beta (Aβ) precursor protein (*App*) locus[36–39]. FAD cases are often linked to autosomal dominant mutations in *App,* and genetic data suggest that APP proteolysis has a central role in both familial and sporadic AD pathogenesis[40,41]. Given that aggregated forms of Aβ are widely considered the primary pathogenic factor in AD (whether sporadic, 95% of cases, or familial, 5% of cases), we first targeted the study of an App^{S} model. Furthermore, the rat has been the organism of choice for most behavioral, memory, and cognitive research, as the rat is an intelligent and quick learner[42], with key biobehavioral processes that are similar in rats and humans. Furthermore, rats have the same tau isoforms as humans (unlike the mouse)[43] and tend to survive to adulthood with homozygous mutations to AD gene targets that can be lethal in mice (e.g., for *Psen1*)[39,44]. Rat and human APP differ by 3 amino-acids in the Aβ region, and human Aβ may have a higher propensity than rodent Aβ to form yet-to-be-identified toxic forms of Aβ, which compelled the generation of a "humanized" rat Aβ component sequence (App^{h}) complement to the App^{S} model. Indeed, a FAD rat model with imposed genetic risk offers a valuable opportunity to identify very early signatures of AD prodromal to characteristic tau and/or amyloid pathology. The App^{S} rat does not consistently develop characteristic AD-like pathology until older age or with additional disease mutations[45,46], despite reported APP pathogenic processing and changes in synaptic signaling across the lifespan compared to humanized controls[36–38]. Therefore, ABRs from App^{S} rats were investigated here in contrast to the appropriate control rat, the knock-in animal with "humanized" mutations, App^{h}, to model the mid-life modifiable risk context that in humans occurs without classical AD pathology[47].

Thus, we seized the opportunity in a preclinical model without overt neuropathology to determine whether a sound-evoked neurophysiological signal could screen known genetic risk for AD between the *App* Swedish risk variant vs. humanized knock-in rats, track risk severity, and detect the effects of intervention—possibly independent of Aβ deposition[46,48]. Comparing conditions with expected differences in APP pathogenic processing opens a unique window to reveal the diagnostic potential of functional synaptic pathological mechanisms of neurodegeneration that are prodromal to amyloid or tau pathology, emerging very early in life and accessible via the auditory system.

RESULTS

Single trials of tone-evoked ABRs were collected (512 repetitions of 5 msec, 5.0 kHz pure tones at 70 dB SPL; 21 Hz repetition rate) in male and female homozygous App^{S} or App^{h} rats.

Hearing thresholds were considered normal and not different between genotypes (*App*^{S} hearing threshold: 42.14 ± 1.84 dB SPL vs. *App*^{H} hearing threshold: 45 ± 2.23 dB SPL, t (8.631) = 0.986, p = 0.351; Welch's *t*-test). However, they were different between sexes (male hearing thresholds: 50 ± 0 dB SPL vs. female hearing thresholds: 41.11 ± 1.11 dB SPL, t (8) = 8.00, p < 0.0001; Welch's *t*-test). Thresholds increased slightly with aging, as expected (5 months old: 40 ± 1.29 dB SPL vs. 12+ months old: 46.67 ± 1.67 dB SPL, t (10) = 3.162, p = 0.010; unpaired t-test). Single-trial ABR data were analyzed as a continuous timeseries of "micromovement" peaks, the mathematics of which have been described in detail[34] (Zenodo record 6299560#.Y3las3bMLcs). Briefly, this method was originally developed with inspiration from the timeseries motor movement datasets across repeated trials of reaching (e.g., for objects) but generalized across a multiplicity of biorhythms of the nervous systems (eyes, face, voice, heart, neural signals). By eye, these signals appear smooth and continuous. They however have moment-to-moment variations that over time inform the system of emerging patterns ranging from random and unpredictable, to organized and highly predictable, such that past events inform of future events. As in a moving average, it is possible to empirically determine the mean peaks and valleys in the signals of interest (as opposed to taking a theoretical mean assumed from an *a priori* imposed distribution). Then, as the system senses the stimuli and responds, the response fluctuations relative to the empirically estimated mean can be tracked moment-by-moment. A standardization of these fluctuations to account for possible allometric effects due to anatomical disparities (such as differences in head circumference and end-effectors' lengths across animals) produce the so-called "micromovement spikes". Continuous time series data across trials generates thousands of such micro-peaks whose distribution parameters can be empirically estimated using e.g., maximum likelihood estimation. As an example, plotting the empirical parameters thus estimated with 95% confidence intervals on a parameter space automatically separated the auditory brainstem responses (ABR) in human neonates who went on to develop neurotypically from those with neuro-atypical development[31]. Here, we adapt the methods to neurophysiological ABR data from a rat model of disease risk. It should be understood then that such normalized micro-peaks reflect small fluctuations in neural activations and at a value of 0 represent local mean activity (**FIGURE 1**). Across biophysical signals, the continuous Gamma family of probability distribution functions has proved to be the best fit (in an MLE sense), capturing human maturational[34] and neurodegenerative[49] stages in the form of a scaling power law. ABR "micromovements spikes" likely reflect increased neurophysiological variance in synaptic transmission along the central auditory pathways, which are usually unobservable in standard trial-averaging practices. Importantly, these patterns are specific to each animal but because of the normalization for allometric effects, the distribution parameters of standardized micro-peaks can be compared on the same parameter space across multiple animals. In this way it is not only possible to quantify individual shifts in probability distributions but also to capture automatically self-emerging classes of animals with similar stochastic properties.

Rat ABR micromovement spikes can be well characterized by a Gamma process

The normalized micro-peaks comprising the micro-movement spikes of rat ABR signals, taken trial by trial instead of averaging the waveforms, follow the continuous family of probability

distributions. The Gamma mean and Gamma variance can be used to compute the Gamma noise to signal ratio, giving us a sense of individualized dispersion of the response fluctuations around the local mean response. Using a time window of 10 ms at a sampling resolution of 195200 Hz, we can capture the stochastic shifts of the responses and separate different classes of animals accordingly. Furthermore, we can characterize the individual stochastic shifts and appreciate the outcomes from different stimuli exposure. As in humans, the Gamma parameters can be represented as points on the Gamma parameter plane spanned by the shape and scale (dispersion) of the empirically estimated distribution family. The log-log scatter of points on the Gamma parameter plane also follows a tight linear fit such that as the scale parameter decreases, the shape parameter increases. The shape parameter at 1 is the special case of memoryless exponential distribution, while higher values represent heavy -tailed distributions, and even larger values (> 100) fall along the symmetric, Gaussian-like ranges of the Gamma family. This result has implications for translational rat models attempting to capture stochastic patterns of neurodevelopment or neurodegeneration analogous to those previously quantified in humans using this model (**FIGURE 1**).

ABR micromovements are sensitive to FAD-risk in rats

Aged *App*^{S} rats (>12 months old) clearly separate within sex in 2-dimensional state space from control *App*^{h} (no overlap in 95% confidence intervals) (**FIGURE 2**). Separation is remarkably still evident in an independent cohort of younger animals (5 months old) (only partial overlap in 95% confidence intervals). Notably, aged animals separate further in the same state space, consistent with the interpretation that ABR metrics capture progressive dysfunction with AD risk, e.g., aging-dependent neurodegeneration (**FIGURE 3**). Interestingly, we found that the same parameter dimensions did not separate animals with an alternate risk allele, the LF autosomal dominant risk variant to presenilin (*Psen1)* that encodes a γ-secretase component linked to familial AD (**SUPPLEMENTARY FIGURE S1**), which suggests that functional differences could be specific to risk genotype. That ABR data separate AD risk and severity is exciting because ABR biometrics may be useful to stratify AD/ADRD by root cause (e.g., to specific disease-generating mutations) that could be important for clinical translation to inform precision medicine tailored to cause and severity.

ABR micromovements normalize after a bout of auditory-cognitive training

Tracked longitudinally, we report that the ABR of *App*^{S} rats can normalize with sound-guided cognitive training to overlap with *App*^{h} (**FIGURE 4**). Remarkably, just a few weeks of directed auditory training in a simple tone-reward task ameliorates this neural processing difference, normalizing auditory responses to become indistinguishable from controls, and persists for at least 9 months (as long as recordings were possible). An initial analysis from the same data shows no differences in hearing thresholds with training (pre-training: 56.67 ± 3.33 dB SPL vs. post-training: 58.33 ± 4.01 dB SPL, $t(5) = 1.00$, $p = 0.363$; paired t-test), yet pre- vs. post-training ABRs from *App*^{S} vs *App*^{h} trained rats show that the amplitude of the second peak wave (PW2) of the

ABR (see **SUPPLEMENTARY FIGURE S3C**) increases with the success of tone-reward memory formation (Pearson's correlation, two-tailed: R = 0.790; p = 0.0197).

DISCUSSION

We report three major findings: First, the rat ABR micromovement spikes are well fit by the continuous Gamma family of probability distributions such that the shape and scale parameters can be used to represent individual animals and cohorts of animals on the Gamma parameter plane. As in humans, the log-log representation follows a tight lineal relation in the form of a scaling power law whereby as the Gamma scale parameter decreases, the shape parameter increases towards the Gaussian ranges of the Gamma family. The range of distributions of this family thus can be used to characterize the distribution ranges for each animal and those of different classes of animals, including as they shift with aging and treatments. In simplest terms, this finding shows a promising case of reverse translation opportune for bridging clinical studies to preclinical models well-suited for development of novel therapeutics or diagnostics. Because of the tight linear relationship between these two parameters defining the continuous Gamma family, knowing one parameter enables us to infer the other, such that we can reduce the representation of data. This is an important feature of novel analytical tools, particularly when training machine learning models and artificial neural networks to automate classification and tracking of disease progression and/or progression with treatments in both preclinical and clinical contexts. Second, ABR micromovements are sensitive to human FAD-risk in both male and female rats, which could render them useful as a sensitive biomarker of AD risk very early in human life, including for tracking disease risk severity with aging. The translational potential of a diagnostic ABR biomarker is high, as it is a rapidly acquired, pre-attentive signal collected non-invasively, which eliminates the need for prolonged or effortful subject engagement, which might be challenging in some clinical populations. Third, we report that ABR micromovement spikes are susceptible to intervention, likely via an experience-dependent neuroplasticity mechanism. Our focus on auditory neurophysiology in rats without hearing loss may raise a question about cochlear synaptopathy despite normal pure-tone thresholds that would preclude the ability to interpret effects on central auditory processing. However, it is unlikely that mutant rats had cochlear dysfunction, given the rescue of the ABR phenotype following cognitive training.

The emergence of a "healthy" ABR state after a bout of auditory-cognitive training, despite the maintained genetic risk in *App*^{S}, suggests that a central neural mechanism can reasonably promote functional resilience. An important consideration for interpreting the training intervention-induced effects is that, even though persistent, they are not expected to reverse or prevent AD-related neurodegeneration or cognitive decline. Rather, this finding provides insight into the underlying neurobiology affected in both hearing function and dementia risk. Further investigation into the mechanisms underlying experience-dependent changes during intervention might have promise for harnessing them to apply more broadly to mitigate AD risk. Altogether, these findings are consistent with the common cause hypothesis for the relationship between hearing and AD/ADRD rooted in a novel functional synaptic pathology that is observable in neurophysiological recordings of evoked brain activity.

ABR micromovement spikes are a potential biomarker for disease risk. This is striking in the *App*^{S} rat because KI rats make no preconceived assumption about the pathogenic mechanisms nor the behavioral consequences of the knocked-in variants; only the unbiased genetic one[46]. In contrast, transgenic models, which produce, e.g., high levels of Aβ and can readily deposit amyloid plaques, are based on the hypothesis that plaques and/or other forms of toxic Aβ have a central pathogenic role in AD. Because there are known human cases where plaques can be present without dementia (e.g., in people who have other protective mutations, such as *ApoE2*), and importantly, plaques and tangles are not present in mid-life, when hearing becomes a major risk factor. Therefore, KI models may be the way of the future for hopeful lines of research to best explain the very early mid-life biological links between hearing and ADRD, independent of the amyloid cascade and/or tau pathology[50]. Consistent with the apparent functional synaptic outcome we report from the auditory system, the *App*^{S} rat has glutamate/GABA transmission imbalances[36,38] that are now becoming more appreciated in AD/ADRD with relevance to pathogenesis (e.g., OFC, entorhinal cortex, hippocampus). The relevance of ABR neurophysiology to potential cognitive phenotypes is supported by recent work in wildtype rats, showing that early ABR waves have “memory effects” that correlate with learning-induced cortical changes related to successful memory formation. The larger the change in ABR Wave amplitudes, and the larger the change in cortical tuning, and behavioral memory[1], extending to experience-dependent plasticity related to early life stress. These ABR findings and others, including those that investigate the complex sound-evoked frequency following response (FFR)[19,23,53,53,54] are consistent with memory-mediated descending cortical control on more peripheral auditory structures of the auditory system that can impose a cognitive structure on earlier neural processing in the auditory pathway to dynamically and adaptively mediate our listening abilities over a lifetime.

Overall, the potential for ABR micromovement spikes as a biomarker in neurodegenerative disease complements work emerging in neurodevelopmental studies that underscore the utility of the central auditory nervous system as a convenient neurophysiological window into early indications of progressive dysfunction in the brain across the lifespan. Characteristic features of the population dynamics of sound-evoked ABRs identified in the current report may provide early, non-invasive biomarkers for detecting the severity of AD risk, and may also offer a readout to stratify AD based on root causes, such as specific disease-generating mutations. It is important to note that the select distinguishing features of multiparametric characteristics are generated by disease-relevant population data, which enables biomarker specificity between disease states (e.g., autism vs. dementia) and root cause within disease states (e.g., APP vs. PSEN1 causing FAD mutations). Leveraging sensitivity and specificity with early detection could enable timely, tailored strategies for precision medicine tailored to the underlying etiology and severity of disease. The field is now poised for future studies to use ABRs to characterize functional synaptic neuropathology in other preclinical and clinical models of neurodegenerative disease, including ADRD related to environmental exposures or sporadic cases, and longitudinal studies that can track susceptibility or resilience in parallel with cognitive phenotyping. Neurophysiological signatures that selectively distinguish dementia risk will provide insights on novel etiologies to stratify AD/ADRD beyond classic clinical hallmarks for applying to next-generation human precision medicine.

SUPPLEMENTAL METHODS

Subjects

Subjects were living, age-matched, male and female CRISPR-mediated knock-in rats aged 4-5 months or 12-24 months old. Rats harbored either a homozygous familial Alzheimer's Disease (AD) Swedish risk variant knocked into the amyloid precursor protein (*App*) locus, or a humanized form of *App* as non-AD risk controls. Homozygous App^S or App^H rats carry two copies of the human Swedish risk mutation or humanized variant, respectively[36] (N=3 per genotype X age). An independent cohort of aged, 12-month-old rats (N=5) modelled an alternate familial AD risk variant to the presenilin-1 (*Psen1*) locus. $Psen1^{LF}$ rats[39] were homozygous for the risk variant mutation to *Psen1*. All animals were individually housed in a colony room with a 12-hr light/dark cycle. Throughout behavioral training procedures only, rats were water-restricted, with daily supplements provided to maintain an ~85 % free-drinking weight. All procedures were approved and conducted in accordance with guidelines by the Institutional Animal Care and Use Committee at Rutgers, The State University of New Jersey (#PROTO999900026 to K.M.B.), performed in accordance with relevant named guidelines and regulations, and reported in compliance with ARRIVE guidelines.

Auditory brainstem response recordings

Auditory brainstem responses (ABRs) were recorded twice in anesthetized rats (ketamine-xylazine, K: 40 mg/kg, X:4 mg/kg, i.p.): (1) Twenty-four hours prior to the first *two-tone* discrimination task (2TD) training session and (2) Twenty-four hours following the final 2TD training session. Single-trial ABR data were recorded (Medusa4Z, TDT Inc.) by an experimenter blind to genotype using automated software (BioSigRZ, TDT Inc.) for data collection using three minimally invasive subdermal electrodes (1 kΩ) positioned at the midline along the head (recording), immediately below the left pinna (reference), and 1 cm posterior from the recording electrode (ground). Sound stimuli were 70 dB SPL, 5 msec, 5 kHz pure-tones (2 msec cosine-gated rise/fall time) presented via a calibrated electromagnetic speaker (MF1; TDT) at 21 Hz to the right ear from a speaker positioned 4 cm away. Tone evoked single trial data (512 trials) analyzed by using mathematical modeling of the distributions of single trial variability across 100s of repeated sound presentations, the mathematics of which have been described in detail[31,34] and scripts available for analysis on Zenodo (record 6299560#.Y3las3bMLcs).

The sound-evoked ABR responses were used to estimate hearing thresholds by sound level, and to analyze the second wave of the ABR (PW2), which appears as a positive peak of the trial-averaged waveform, and is reliably observed in both naïve and trained rats[51,55]. Hearing threshold was defined using trial-averaged ABR traces for each animal as the lowest sound level that elicited a visually identifiable ABR waveform (**SUPPLEMENTARY FIGURE S2**) and confirmed by at least two independent human raters. The resulting ABR thresholds (dB SPL) were compared using unpaired t-tests with Welch's correction ($\alpha = 0.05$) for between-group analyses (genotype, sex, and age) and paired t-tests ($\alpha = 0.05$) for within-group comparisons (trained vs. untrained) App^S and App^H *rats.* Custom Matlab scripts were used to identify peaks within the waveform and to derive the trough-to-peak amplitude (nV) of wave peaks in the trial-averaged ABR. The second peak (PW2) amplitude was measured to determine training intervention-induced effects changes between the App^S and App^H groups using previously published

methods[51,55]. Peak amplitude was defined as the voltage difference between the preceding trough and the peak (**SUPPLEMENTARY FIGURE S3**). Pearson correlation analyses were used to assess relationships between the PW2 amplitude and the success of tone-reward memory formation (see **Behavioral analysis** below). All statistical analyses were performed using GraphPad Prism software (Boston, Massachusetts, USA).

Single-trial timeseries data analysis

A continuous timeseries of trial-by-trial micromovements, which are small fluctuations in neural activations within each ABR trial, was used to construct a multidimensional parameter space for subsequent analysis. Fluctuations occurring before and after the sound-evoked ABR peak, which are typically discarded in conventional trial-averaging approaches, were retained to capture additional signal variability. This underutilized information in the rich ABR response is used to build standardized waveforms that are normalized by computing deviations from the mean amplitude, standardizing traces across individuals, and controlling for neuroanatomical variability. Time-stamped microvariations, as recorded by the data acquisition system, were then subjected to empirical estimation of the probability distribution function (PDF) to determine the best-fitting distribution parameters that characterize the observed fluctuations. The Gamma (the best fit for peaks' features, such as amplitude and timing) parameter plane spanned by the shape and scale parameters is plotted with 95% confidence intervals for each estimated shape and scale value. This approach enabled optimal feature extraction and the derivation of interpretable parameter spaces for downstream comparisons between individuals or experimental groups. The percentage of overlap in multivariate state space—analogous to principal component analysis (PCA)—was used as a quantitative measure of separation between genotypes (e.g., 0% overlap indicating strong discrimination and an excellent diagnostic biometric; 100% indicating no separation and a poor diagnostic biometric) or learning states (e.g., pre- vs. post-training). Significant amplitude differences as a function of learning were evaluated using paired t-tests.

Behavioral procedures

All behavioral training and test sessions were conducted in instrumental conditioning chambers within a sound-attenuated box. All rats were water-restricted and initially trained to bar press for water reward in five ~45-min bar-press shaping sessions before beginning the experimental timeline shown in **SUPPLEMENTARY FIGURE S4**. This phase of training ensured that all animals could acquire the procedural aspects of the task (i.e., bar-pressing for rewards) before any sounds were introduced. Next, rats were trained to bar press (BP) to pure tones for water rewards in a *two-tone* discrimination task (2TD). Responses to a target pure tone frequency (S+, 5.0 kHz; 75 dB SPL, 8 s) resulted in reward, while responses to the non-target (S-, 11.5 kHz; 75 dB SPL, 8 s) were unrewarded and triggered an error signal (flashing house light) and a "time-out" (an extended 6 s interval until the start of the next trial). Inter-trial intervals (ITIs) were, on average, 8 s (range: 4–12 s, randomized). BPs during an ITI were inconsequential (i.e., no time-out, no reward). Sessions were consecutive, daily, and 30 minutes in length.

Behavioral analysis

Daily 2TD performance was calculated as the number of bar presses (BP) to the rewarded tone (S +) divided by the number of bar presses to both the S+ and unrewarded tone (S−) as follows: $P = 100\% \times [\#BP^{S+} / (BP^{S+} + \#BP^{S-})]$. 2TD training continued until rats reached a criterion performance asymptote for 3 consecutive days (or a maximum of 20 training sessions). The performance asymptote criterion was defined by the combination of: (1) performance ≥70%, (2) ≤10% coefficient of variation, and (3) $[(\# BP^{S+} / \#Trials^{S+}) - (\# BP^{S-} / \# Trials^{S-})] / [(\# BP^{S+} / \# Trials^{S+}) + (\# BP^{S-} / \# Trials^{S-})] \geq 1$. It is important to note that the 2TD task is not difficult perceptually since the acoustic frequencies are over an octave apart and easily distinguished by naïve rodents[56]. Rather, the behavioral challenge was associative in nature: 2TD performance demands the formation of memory for which tone frequency is associated with reward (vs. no reward).

Twenty-four hours following the final 2TD training session, rats were given a tone memory test to determine the success of auditory memory formation after 2TD training. During the memory test, rats were presented with a range of sound frequencies, including the S+ and S− frequencies 10 different pure tone frequencies were tested: 3.6, 4.2, 5.0 (S+ rewarded tone), 5.9, 7.0, 8.3, 9.7, 11.5 (S− unrewarded tone), 13.6, and 16.0 kHz (all pure tones presented at a sound level of 75 dB SPL). Test tones neighbored the S+ or S− spaced at a distance of ∼1/4 octave. The tone memory test began with 15 regular trials of the 2TD task (BPs to the S+ are rewarded; BPs to the S− are not) to confirm stable performance on the day of the memory test[57]. Each tone frequency was presented a total of 8 times. The session was divided into two continuous blocks, with two presentations of each tone per block in a pseudorandom order. No responses were reinforced. The number and latency of behavioral responses to test tones were used to determine the shape of frequency generalization gradients around the two signal frequencies. The number of BPs made during the tone memory test for each test frequency was expressed as a proportion of the total number of BPs made by an individual animal. These proportions were then averaged across animals within each group (App^S and App^H) to obtain group means for each test frequency. To quantify the success of tone-reward memory formation for the rewarded signal tone, a tone memory index was calculated as the percentage of responses to the rewarded signal tone (5.0 kHz) – percentage of responses to a single neighbor tone (5.9 kHz), which that matches the sound frequencies used in auditory brainstem response recordings. Positive values indicate greater responding to the rewarded signal tone than the nearby neighbor tone.

The following measures were used for Pearson correlation analyses. For behavioral measures, tone memory specificity was defined as the difference in percentage of bar-presses to 5.0 kHz vs. 5.9 kHz. For ABR data, first, PW2 amplitude evoked by the rewarded tone (5.0 kHz) and a single neighbor tone (5.9 kHz) were identified using custom Matlab scripts for each subject as described in detail[55]. Then contrast measures for the difference in PW2 amplitude between ABRs evoked by 5.0 vs. 5.9 kHz following a simple sound-reward go/no-go learning task were calculated for each subject. To assess training intervention-induced effects, the PW2 amplitude was identified using ABRs recorded ABRs recorded 24 h following the tone memory test. Finally, Pearson correlation analysis was used to evaluate the relationship between training intervention-induced changes in differences in PW2 amplitude of 5.0 kHz vs 5.9 kHz and the difference in percentage of responses made to the 5.0 kHz tone vs 5.9 kHz during the Memory Test as previously[51,55].

Inclusion and Exclusion Criteria

All rats underwent a screening phase for inclusion in the single-trial ABR timeseries datasets to ensure the reliability of single-trial data acquired across the entire duration of the recording session for accurate within-animal phenotyping and generalizability of the results across the group. To do so, we divided continuous timeseries data within each individual subject into 8 equal epochs and estimated the trajectory of data distribution and confidence intervals of the measured parameters within the subject's recording session. A Noise-to-Signal Ratio (NSR) was then calculated by dividing the variance of the electrophysiological signal by its mean. This approach allowed us to determine within-animal trajectories reflecting the consistency of data acquired within the same recording session, to assess changes in distributional characteristics, and compare these patterns across rats within the same experimental group (e.g., genotype). One rat (female App^{S}) exhibited a markedly different NSR trend from the rest of the group by showing an orthogonal trajectory and was a clear outlier of the group profile. To prevent a reduction in the generalizability of our results, this rat was excluded from analysis. An additional rat (female App^{H}) showed aberrant behavior, so was also excluded from analysis. In total, data from 17 of 19 rats studied were included. All screening procedures were conducted blind to genotype and sex.

Data and analytical code availability

Data and code are available in a Zenodo data repository.

REFERENCES

1. Panza, F. *et al.* Age-related hearing impairment and frailty in Alzheimer's disease: interconnected associations and mechanisms. *Front. Aging Neurosci.* **7**, (2015).

2. Lin, F. R. *et al.* Hearing Loss and Incident Dementia. *Arch. Neurol.* **68**, (2011).

3. Livingston, G. *et al.* Dementia prevention, intervention, and care. *The Lancet* **390**, 2673–2734 (2017).

4. Taljaard, D. S., Olaithe, M., Brennan-Jones, C. G., Eikelboom, R. H. & Bucks, R. S. The relationship between hearing impairment and cognitive function: a meta-analysis in adults. *Clin. Otolaryngol.* **41**, 718–729 (2016).

5. Mamo, S. K. *et al.* Hearing Care Intervention for Persons with Dementia: A Pilot Study. *Am. J. Geriatr. Psychiatry* **25**, 91–101 (2017).

6. Maharani, A. *et al.* Longitudinal Relationship Between Hearing Aid Use and Cognitive Function in Older Americans. *J. Am. Geriatr. Soc.* **66**, 1130–1136 (2018).

7. Dawes, P. *et al.* Hearing Loss and Cognition: The Role of Hearing Aids, Social Isolation and Depression. *PLOS ONE* **10**, e0119616 (2015).

8. Lin, F. R. & Albert, M. Hearing Loss and Dementia – Who's Listening? *Aging Ment. Health* **18**, 671–673 (2014).

9. Lin, F. R. *et al.* Hearing intervention versus health education control to reduce cognitive decline in older adults with hearing loss in the USA (ACHIEVE): a multicentre, randomised controlled trial. *Lancet Lond. Engl.* **402**, 786–797 (2023).

10. Reed, N. S. *et al.* Recruitment and baseline data of the Aging and Cognitive Health Evaluation in Elders (ACHIEVE) study: A randomized trial of a hearing loss intervention for reducing cognitive decline. *Alzheimers Dement. N. Y. N* **10**, e12453 (2024).

11. Weinberger, N. M. & Bieszczad, K. M. Introduction: From Traditional Fixed Cortical Sensationism to Contemporary Plasticity of Primary Sensory Cortical Representations. in *Neurobiology of Sensation and Reward* (ed. Gottfried, J. A.) (CRC Press/Taylor & Francis, Boca Raton (FL), 2011).

12. Bieszczad, K. M. & Weinberger, N. M. Representational gain in cortical area underlies increase of memory strength. *Proc. Natl. Acad. Sci. U. S. A.* **107**, 3793–3798 (2010).

13. Bieszczad, K. M. & Weinberger, N. M. Extinction reveals that primary sensory cortex predicts reinforcement outcome. *Eur. J. Neurosci.* **35**, 598–613 (2012).

14. Schreiner, C. E. & Polley, D. B. Auditory map plasticity: diversity in causes and consequences. *Curr. Opin. Neurobiol.* **24**, 143–156 (2014).

15. Pienkowski, M. & Eggermont, J. J. Cortical tonotopic map plasticity and behavior. *Neurosci. Biobehav. Rev.* **35**, 2117–2128 (2011).

16. McGann, J. P. Associative learning and sensory neuroplasticity: how does it happen and what is it good for? *Learn. Mem. Cold Spring Harb. N* **22**, 567–576 (2015).

17. Noda, T., Aschauer, D. F., Chambers, A. R., Seiler, J. P.-H. & Rumpel, S. Representational maps in the brain: concepts, approaches, and applications. *Front. Cell. Neurosci.* **18**, 1366200 (2024).

18. Coomes Peterson, D. & Schofield, B. R. Projections from auditory cortex contact ascending pathways that originate in the superior olive and inferior colliculus. *Hear. Res.* **232**, 67–77 (2007).

19. Chandrasekaran, B., Skoe, E. & Kraus, N. An integrative model of subcortical auditory plasticity. *Brain Topogr.* **27**, 539–552 (2014).

20. Asilador, A. & Llano, D. A. Top-Down Inference in the Auditory System: Potential Roles for Corticofugal Projections. *Front. Neural Circuits* **14**, 615259 (2020).

21. Antunes, F. M. & Malmierca, M. S. Corticothalamic Pathways in Auditory Processing: Recent Advances and Insights From Other Sensory Systems. *Front. Neural Circuits* **15**, 721186 (2021).

22. Fritz, J., Elhilali, M. & Shamma, S. Active listening: task-dependent plasticity of spectrotemporal receptive fields in primary auditory cortex. *Hear. Res.* **206**, 159–176 (2005).

23. Kraus, N. & White-Schwoch, T. Unraveling the biology of auditory learning: A cognitive-sensorimotor-reward framework. *Trends Cogn. Sci.* **19**, 642–654 (2015).

24. Fu, V. X. *et al.* Perception of auditory stimuli during general anesthesia and its effects on patient outcomes: a systematic review and meta-analysis. *Can. J. Anaesth. J. Can. Anesth.* **68**, 1231–1253 (2021).

25. Lesicko, A. M. H. & Geffen, M. N. Diverse functions of the auditory cortico-collicular pathway. *Hear. Res.* **425**, 108488 (2022).

26. Gates, G. A., Anderson, M. L., Feeney, M. P., McCurry, S. M. & Larson, E. B. Central Auditory Dysfunction in Older People with Memory Impairment or Alzheimer's Dementia. *Arch. Otolaryngol. Head Neck Surg.* **134**, 771–777 (2008).

27. Johnson, J. C. S. *et al.* Hearing and dementia: from ears to brain. *Brain J. Neurol.* **144**, 391–401 (2021).

28. Parkkonen, L., Fujiki, N. & Mäkelä, J. P. Sources of auditory brainstem responses revisited: Contribution by magnetoencephalography. *Hum. Brain Mapp.* **30**, 1772–1782 (2009).

29. Skoe, E. & Chandrasekaran, B. The layering of auditory experiences in driving experience-dependent subcortical plasticity. *Hear. Res.* **311**, 36–48 (2014).

30. Kraus, N. *et al.* Subconcussion revealed by sound processing in the brain. *Exerc. Sport Mov.* **1**, 1–4 (2023).

31. Torres, E. B. *et al.* Sensing echoes: temporal misalignment in auditory brainstem responses as the earliest marker of neurodevelopmental derailment. *PNAS Nexus* **2**, 315 (2023).

32. Patel, S. P. *et al.* Neural Processing of Speech Sounds in ASD and First-Degree Relatives. *J. Autism Dev. Disord.* **53**, 3257–3271 (2023).

33. Tarawneh, H. Y., Mulders, W. H. A. M., Sohrabi, H. R., Martins, R. N. & Jayakody, D. M. P. Investigating Auditory Electrophysiological Measures of Participants with Mild Cognitive Impairment and Alzheimer's Disease: A Systematic Review and Meta-Analysis of Event-Related Potential Studies. *J. Alzheimers Dis. JAD* **84**, 419–448 (2021).

34. Torres, E. B. *et al.* Autism: the micro-movement perspective. *Front. Integr. Neurosci.* **7**, 32 (2013).

35. Vidler, M. & Parkert, D. Auditory brainstem response threshold estimation: subjective threshold estimation by experienced clinicians in a computer simulation of the clinical test. *Int. J. Audiol.* **43**, 417–429 (2004).

36. Tambini, M. D., Yao, W. & D'Adamio, L. Facilitation of glutamate, but not GABA, release in Familial Alzheimer's APP mutant Knock-in rats with increased β-cleavage of APP. *Aging Cell* **18**, e13033 (2019).

37. Tambini, M. D., Norris, K. A. & D'Adamio, L. Opposite changes in APP processing and human Aβ levels in rats carrying either a protective or a pathogenic APP mutation. *eLife* **9**, e52612.

38. Yesiltepe, M. *et al.* Late-long-term potentiation magnitude, but not Aβ levels and amyloid pathology, is associated with behavioral performance in a rat knock-in model of Alzheimer disease. *Front. Aging Neurosci.* **14**, 1040576 (2022).

39. Tambini, M. D. & D'Adamio, L. Knock-in rats with homozygous PSEN1L435F Alzheimer mutation are viable and show selective γ-secretase activity loss causing low Aβ40/42 and high Aβ43. *J. Biol. Chem.* **295**, 7442–7451 (2020).

40. Bayer, T. A., Cappai, R., Masters, C. L., Beyreuther, K. & Multhaup, G. It all sticks together--the APP-related family of proteins and Alzheimer's disease. *Mol. Psychiatry* **4**, 524–528 (1999).

41. van der Kant, R. & Goldstein, L. S. B. Cellular functions of the amyloid precursor protein from development to dementia. *Dev. Cell* **32**, 502–515 (2015).

42. Foote, A. L. & Crystal, J. D. Metacognition in the rat. *Curr. Biol. CB* **17**, 551–555 (2007).

43. Hanes, J. *et al.* Rat tau proteome consists of six tau isoforms: implication for animal models of human tauopathies. *J. Neurochem.* **108**, 1167–1176 (2009).

44. Xia, D. *et al.* Presenilin-1 knockin mice reveal loss-of-function mechanism for familial Alzheimer's disease. *Neuron* **85**, 967–981 (2015).

45. Tambini, M. D. *et al.* Aβ43 levels determine the onset of pathological amyloid deposition. *J. Biol. Chem.* **299**, 104868 (2023).

46. D'Adamio, L. Transfixed by transgenics: how pathology assumptions are slowing progress in Alzheimer's disease and related dementia research. *EMBO Mol. Med.* **15**, e18479 (2023).

47. Livingston, G. *et al.* Dementia prevention, intervention, and care: 2024 report of the Lancet standing Commission. *The Lancet* **404**, 572–628 (2024).

48. van der Kant, R., Goldstein, L. S. B. & Ossenkoppele, R. Amyloid-β-independent regulators of tau pathology in Alzheimer disease. *Nat. Rev. Neurosci.* **21**, 21–35 (2020).

49. Torres, E. B., Caballero, C. & Mistry, S. Aging with Autism Departs Greatly from Typical Aging. *Sensors* **20**, 572 (2020).

50. Yesiltepe, M., Yin, T. & D'Adamio, L. Beyond amyloid: altered gene function in neurodegenerative diseases. *Aging* **15**, 9235–9237 (2023).

51. Rotondo, E. K. & Bieszczad, K. M. Precise memory for pure tones is predicted by measures of learning-induced sensory system neurophysiological plasticity at cortical and subcortical levels. *Learn. Mem. Cold Spring Harb. N* **27**, 328–339 (2020).

52. Rotondo, E. K. & Bieszczad, K. M. Memory Specific to Temporal Features of Sound Is Formed by Cue-Selective Enhancements in Temporal Coding Enabled by Inhibition of an Epigenetic Regulator. *J. Neurosci. Off. J. Soc. Neurosci.* **41**, 9192–9209 (2021).

53. Kraus, N., Strait, D. & Parbery-Clark, A. Cognitive factors shape brain networks for auditory skills: spotlight on auditory working memory. *Ann. N. Y. Acad. Sci.* **1252**, 100–107 (2012).

54. Coffey, E. B. J. *et al.* Evolving perspectives on the sources of the frequency-following response. *Nat. Commun.* **10**, 5036 (2019).

55. Rotondo, E. K. & Bieszczad, K. M. Sensory cortical and subcortical auditory neurophysiological changes predict cue-specific extinction behavior enabled by the pharmacological inhibition of an epigenetic regulator during memory formation. *Brain Res. Bull.* **169**, 167–183 (2021).

56. Talwar, S. K. & Gerstein, G. L. Auditory frequency discrimination in the white rat. *Hear. Res.* **126**, 135–150 (1998).

57. Shang, A., Bylipudi, S. & Bieszczad, K. M. Inhibition of histone deacetylase 3 via RGFP966 facilitates cortical plasticity underlying unusually accurate auditory associative cue memory for excitatory and inhibitory cue-reward associations. *Behav. Brain Res.* **356**, 453–469 (2019).

Acknowledgments
We thank Dr. Marc Tambini and Dr. Luciano D'Adamio for their generous gifts of experimental animals and breeder knock-in rats, which supported the establishment of our colony and the completion of this work. We also thank all members of the CLEF Lab at Rutgers University for their continuous insight and valuable input into this project.

Author Contributions
Conceptualization: A.G.A. and K.M.B.; Methodology: A.G.A. and K.M.B.; Investigation: A.G.A.; E.Y., P.M., F.R.; Visualization: A.G.A., E.B.T. and K.M.B.; Data analysis: A.G.A., P.M., F.R., E.Y., S.R., E.B.T. and K.M.B.; Funding acquisition: K.M.B.; Supervision: K.M.B., (computational) E.B.T.; Software: E.B.T.; Writing – original draft: K.M.B. and A.G.A.; Writing—review and editing: A.G.A., E.B.T., and K.M.B. All authors read and approved the manuscript.

Funding
This work was supported by the National Institutes of Health, the National Institute on Deafness and Communication Disorders [R01-DC018561 to K.M.B.] E.B.T. was funded by the Nancy Lurie Marks Family Foundation Career Continuation Award.

Competing interests
The authors declare no competing interests.

FIGURES

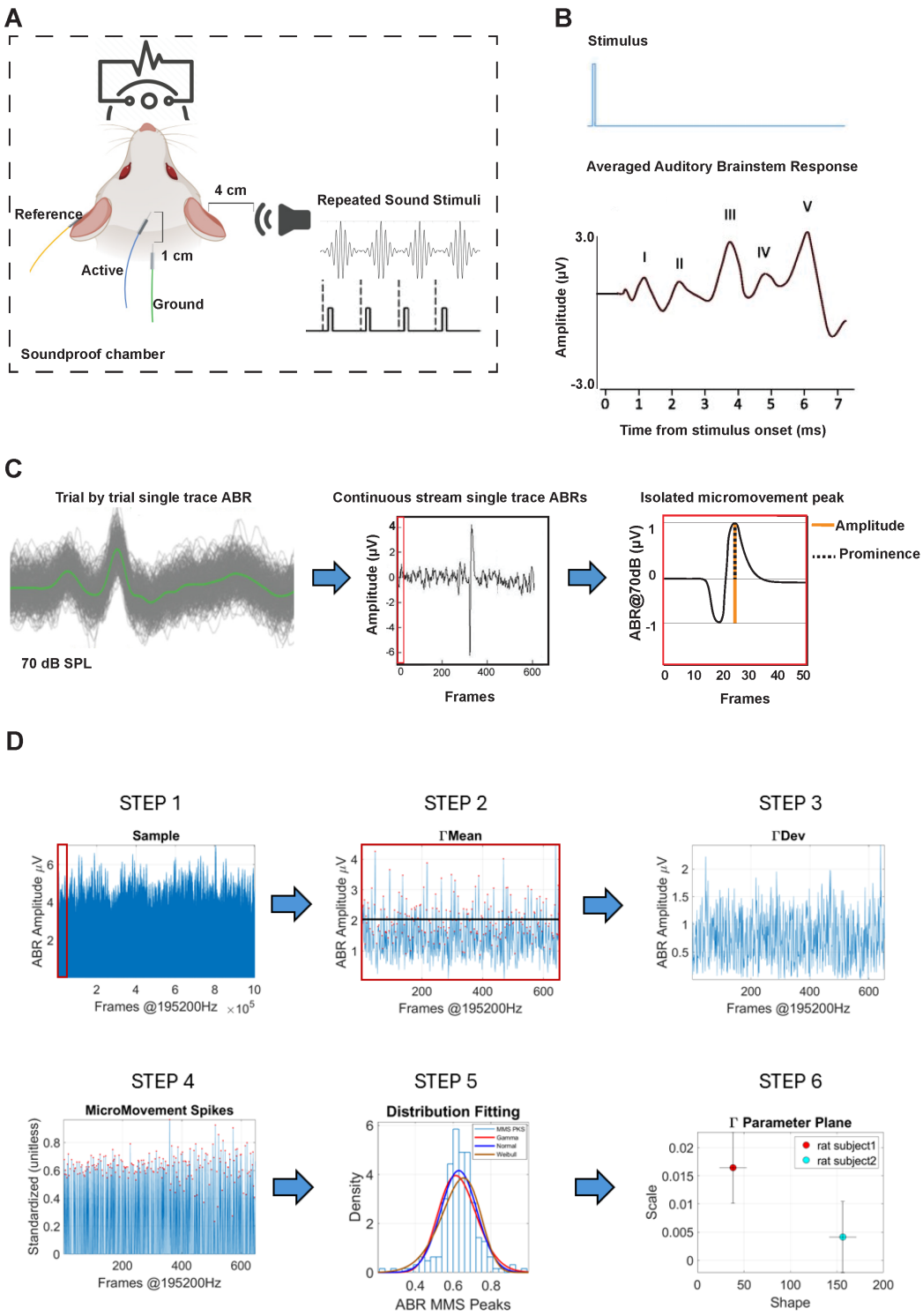

Figure 1: A schematic for auditory brainstem response (ABR) setup and multivariate time-series analysis. **(A)** Rats are anesthetized and three subdermal electrodes are gently applied. The active electrode (blue) is inserted into the scalp subdermally at the vertex of the skull and between the ears. The reference (yellow) and ground (green) electrodes are placed near the mastoid, and 1 cm away

from the active electrode, respectively. A series of repeated tone burst stimuli (5 ms duration (2 ms cosine-gated rise/fall), 5 kHz pure tones at 70 dB SPL, presented at a rate of 21 Hz) is delivered via a magnetic speaker positioned 4 cm from the animal's ear. An anechoic soundproof chamber contains the prepared subject (illustrated as a dotted line) throughout the recording. **(B)** The tone-burst stimulus (top) triggers a time-locked ABR waveform (bottom) that can be averaged across trials to reveal canonical wave peaks. Successive peaks are labeled with Roman numerical I to V. **(C)** *Left:* Repeated epochs of sound-evoked single-trial ABR responses recorded generate thousands of "micromovement" peaks, which generates a distribution that can be analyzed for attributes such as amplitude and prominence, and their means and variance across the micro-peak population. The trial-averaged ABR is shown in green, and the gray traces shows individual single-trial responses as a demonstration of trial-to-trial variability that is traditionally "averaged out" in standard physiological practices. Note the distinction between trial-averaged ABR analyses and those performed here on single-trial ABR data. *Middle:* Single trial ABR data shown as a continuous timeseries across repeated trials is plotted as a stream. *Right:* Zoom-in on a single ABR micromovement peak illustrates different parameters that can be used for physiological characterization, including micro-peak amplitude (red line) and micro-peak prominence (dotted black line). Variations in parameters of interest (e.g. peak amplitudes and prominences) are used to quantify stochastic characteristics. **(D).** Pipeline to derive the micro-movement spikes and Gamma representation from positively rectified ABR signals. *Step 1* is to take the original time series of positive-rectified amplitudes (in microVolts) and obtain windows of activity such as a representative window in *Step 2*. Once the peaks are identified (marked in red dots) we obtain the empirically estimated mean (marked as a black line) and derive in *Step 3* the deviations of the peaks from the mean in *Step 2*. These (absolute) deviations are then subject to *Equation 1* in the main text, to scale out possible allometric effects due to anatomical differences across animals. *Step 4* then provides the micro-movement spikes (MMS) ranging in the real interval [0,1] and providing the standardized signal that enables comparisons across animals and treatments. Here 0 values correspond to mean activity (black line in Step 2). *Step 5* is the Distribution fitting of the MMS peaks (marked with red dots) whereby the continuous Gamma family of probability distribution functions fits the frequency histogram best, in a maximum likelihood (MLE) sense. *Step 6* provides a representation of the data in the Gamma parameter plane spanned by the shape and scale (dispersion) Gamma parameters. Here two representative rat subjects are shown as points on this plane with 95% confidence intervals for each parameter dimension. Their ABR data went through *Steps 1-5* together and show relative physiological dissimilarity in state space. 95% confidence intervales are shown using target marks around mean values. *Abbreviations*: ABR, auditory brainstem response; SPL, sound pressure level.

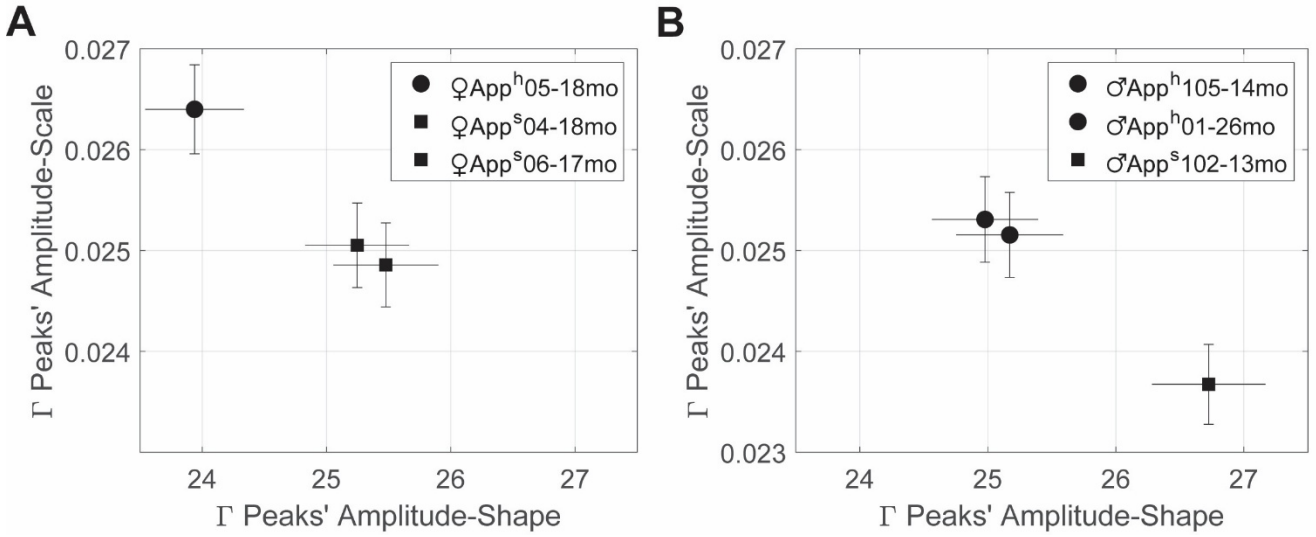

Figure 2: Multivariate time-series analysis of *auditory brainstem response (ABR)* data predicts AD risk in aged rats. ABR response characteristics distinguish AD risk mutant App^S rats (*App* Swedish homozygous, square icons) from App^H controls (*App* humanized allele, circle icons) in a 2-dimensional state space defined by micromovement (gamma), shape (x-axis), and **scale** (y-axis). For (**A**) shows separation in the peaks' amplitude in the ABR waveform for females, and (**B**) shows separation for males. Each symbol represents an individual subject, and error bars indicate within-trial fluctuations in the peak amplitude, shown as 95% confidence intervals (crosshairs). There is 0 % overlap between risk vs. wildtype genotypes in both sexes. Legend shows genotypes. Abbreviation: *App*, amyloid precursor protein.

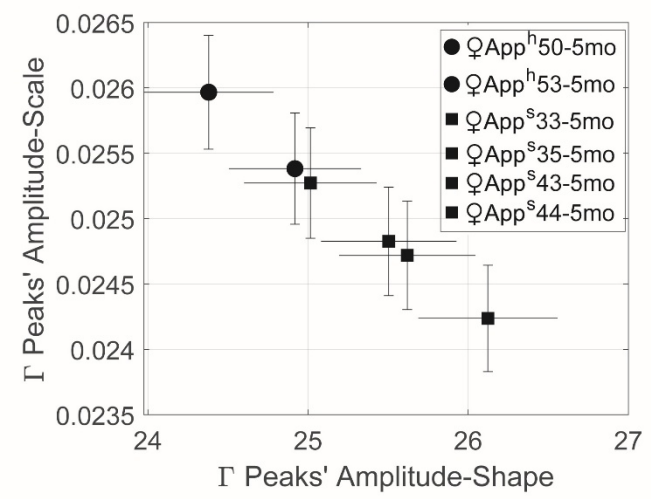

Figure 3: A*uditory brainstem response (ABR)* waveform features capture AD risk in young (5-month-old) female rats. Same as in Fig. 2, but in young age, fluctuations in the peaks' amplitude in the ABR distinguish AD risk mutant female App^S rats (square icons) vs App^H controls (circle icons). Only one App^S rat fails to distinguish from the control subject's confidence space, consistent with individual differences in susceptibilities to geneticallydriven phenotypes. Otherwise, there is a robust separation between AD risk and wildtype genotypes. Points represent the gamma shape and scale parameter space to localize individual subjects with 95% confidence intervals.

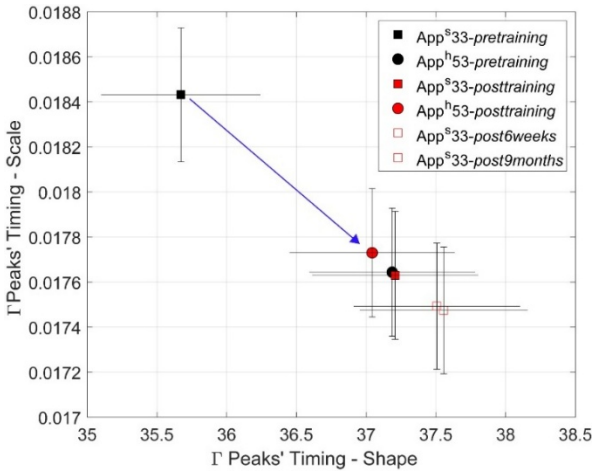

Figure 4: Auditory training shifts *auditory brainstem response (ABR)* waveform dynamics in *App^S* and *App^H* rats and normalizes the auditory responses of *App^S* rats. As before, stochastic patterns of multivariate characteristics in the ABR distinguish AD risk mutant *App^S* rats (square icons) from *App^H* controls (circle icons) in a 2-dimensional state space (gamma shape and scale), which is evident before training (black icons). However, after training the animals in a simple sound-reward go/no-go learning task, there is a functional change that is read out in our ABR metric (red icons). Remarkably, the APP^s ABR is normalized to the *App^H* condition with this intervention (blue arrow shows effect in this space state towards the same >90% overlapping area). This effect on *App^S* lasts at least up to 9 months (open circles show 6 weeks and 9 months post-training). Error bounds show the variability in the relevant parameter of an individual subject's profile in this state space over time as a 95% confidence interval (crosshairs). Data from two female rats are shown, using longitudinal recording of ABRs from each to characterize dramatic shifts induced by training intervention.

SUPPLEMENTARY FIGURES

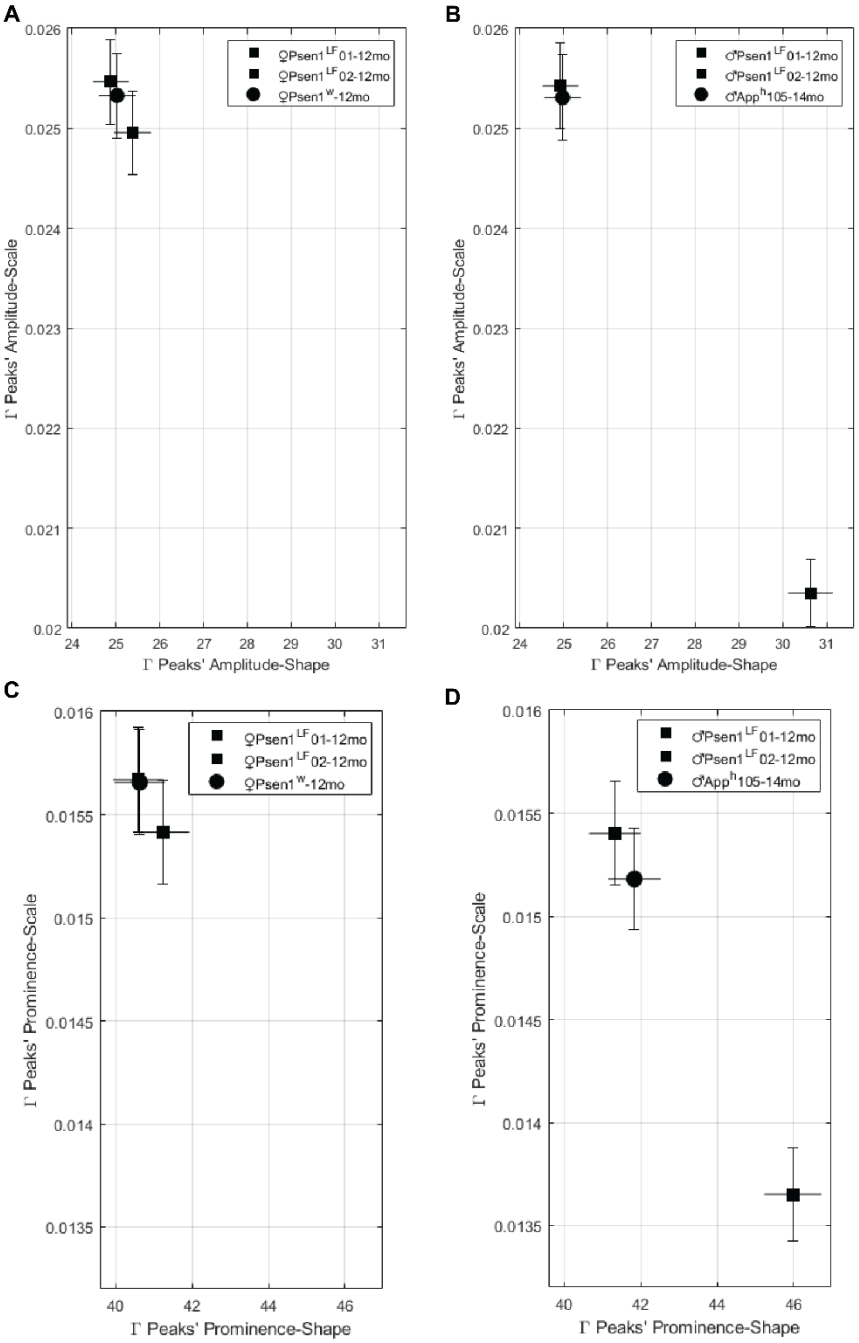

Supplemental Figure S1: *Multiparametric auditory brainstem response (ABR) peak's feature extraction can separate AD risk genotypes and reveal mutation-specific signatures, while preserving within-genotype consistency.* (A- B) Fluctuations in the peaks' amplitude in the ABR fail to separate both female (left) and male (right) *Psen1^{LF}* rats (square icons) from humanized control rats (*Psen1^{w}*, circle icons, right; *App^{H}*, circle icons, left) in a 2-dimensional state space (gamma shape and scale). (C) Changing the variability measures of peak's feature parameter to peaks' prominence (another feature parameter) slightly changes in appearance of overlapping between *Psen1^{LF}* rats (square icons) from *Psen1^{w}* (circle icons), *however, (D) it* reveals separation

between *Psen1*^{LF} rats (square icons) from same humanized control rat (*App*^{H}, circle icons) in B. *The observed separation arises from* unique variability measures and distribution-based statistics derived from ABR responses, highlighting the power of this approach for capturing disease-relevant dynamics. *Note that axes in panels A and B represent different features than those in panels C and D.*

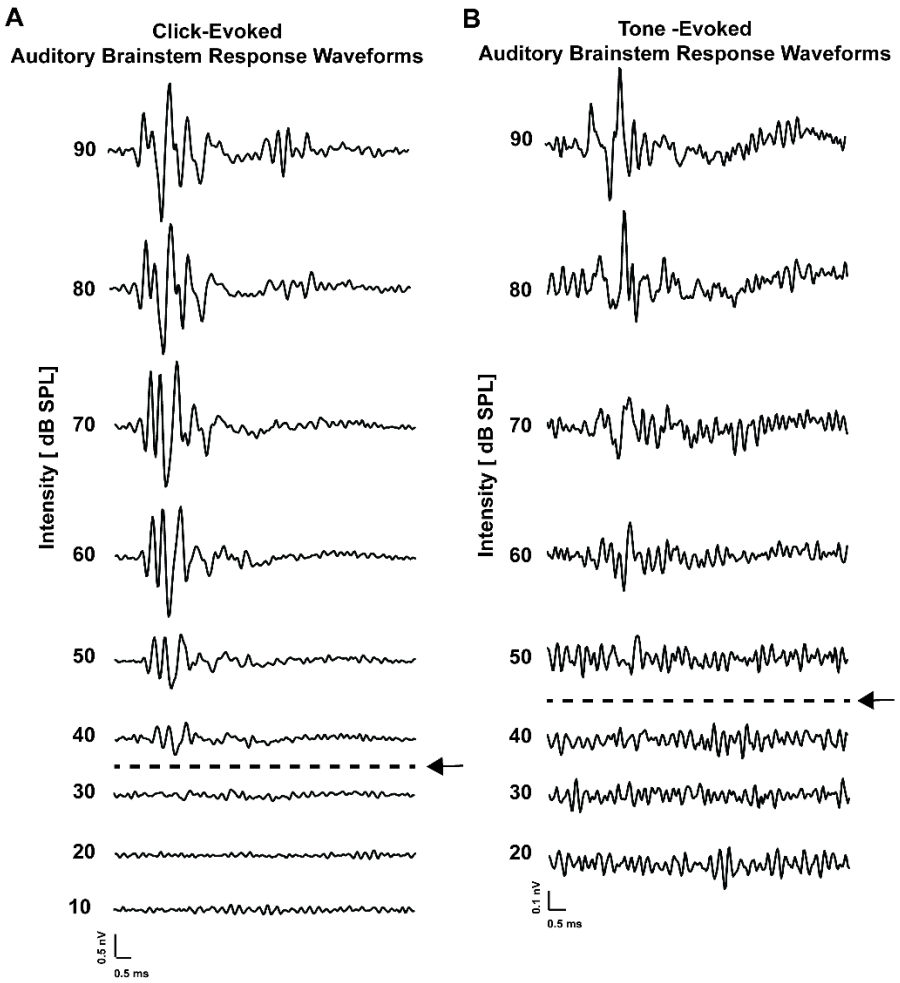

Supplemental Figure S2: *Trial-averaged auditory brainstem response (ABR) traces are used for hearing threshold functional assessment and peak amplitude measurement.* Example of Click- and Tone-Evoked ABRs across sound levels and determination of hearing thresholds. (A) A representative click-evoked ABR waveforms recorded from a 5-month-old female *App*^{S} rat across a range of sound intensities (90–10 dB SPL, decreasing in 10 dB steps; 0–10 ms from stimulus onset). Hearing threshold was determined as 40 dB SPL, the lowest sound level that elicits a characteristic ABR waveform (indicated by the dashed line and arrow). (B) Tone-evoked ABR waveforms recorded from the same animal in response to 5.0 kHz tone bursts presented at intensities ranging from 90 to 20 dB SPL. Tone-evoked ABR waveforms were recorded from the same animal using 5.0 kHz tone burst stimuli at intensities ranging from 90 to 20 dB SPL. The tone-evoked threshold was similarly defined as the lowest sound intensity eliciting a detectable response, which in this case was 50 dB SPL (indicated by the dashed line and arrow). Waveform traces at each sound level represent 512 trial-averaged responses. Abbreviation: SPL, sound pressure level

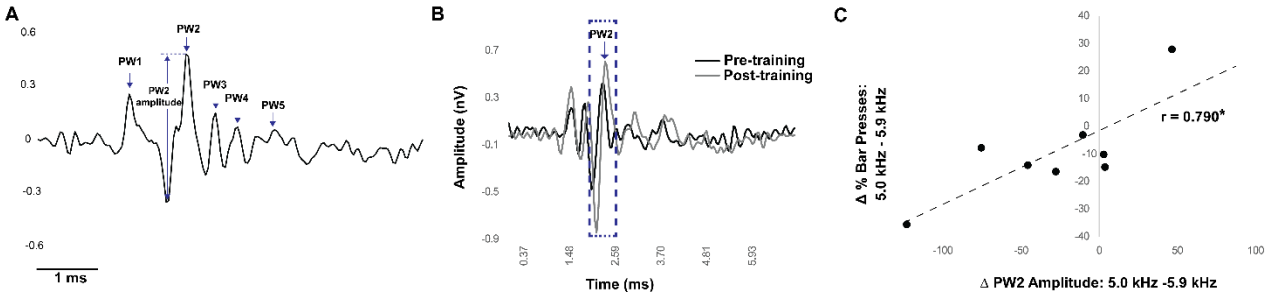

Supplemental Figure S3: *Identification of auditory brainstem response (ABR) peaks and relationship between positive peak 2 (PW2) amplitude change and memory formation.* **(A)** Representative sound-evoked ABR waveform from a rat, showing identified peaks PW1–PW5. The amplitude of a wave is measured in nanovolts (nV) from the peak of a wave to the peak of the next trough. PW2 amplitude is defined as the voltage difference between the preceding trough and the PW2 peak (left). **(B)** Representative ABR traces evoked by the rewarded tone (5.0 kHz) at before ("pre-training," black) and after ("post-training," gray) two tone reward training time points. There was an increase in the PW2 amplitude in ABRs evoked by a rewarded signal tone from pre- to post- two-tone reward training. Dashed boxes indicate PW2. (middle). **(C)** There is a significant positive correlation between differences in PW2 amplitude ABRs evoked by the 5.0 kHz signal tone vs. a nearby neighbor tone (5.9 kHz) and the difference in percentage of responses made to the 5.0 kHz tone vs 5.9 kHz during the memory test. Dots indicate individual data points. Greater amplitude differences predict a greater difference in the percentage of responses allocated to the signal tone frequency. (*) $P < 0.05$ (right).

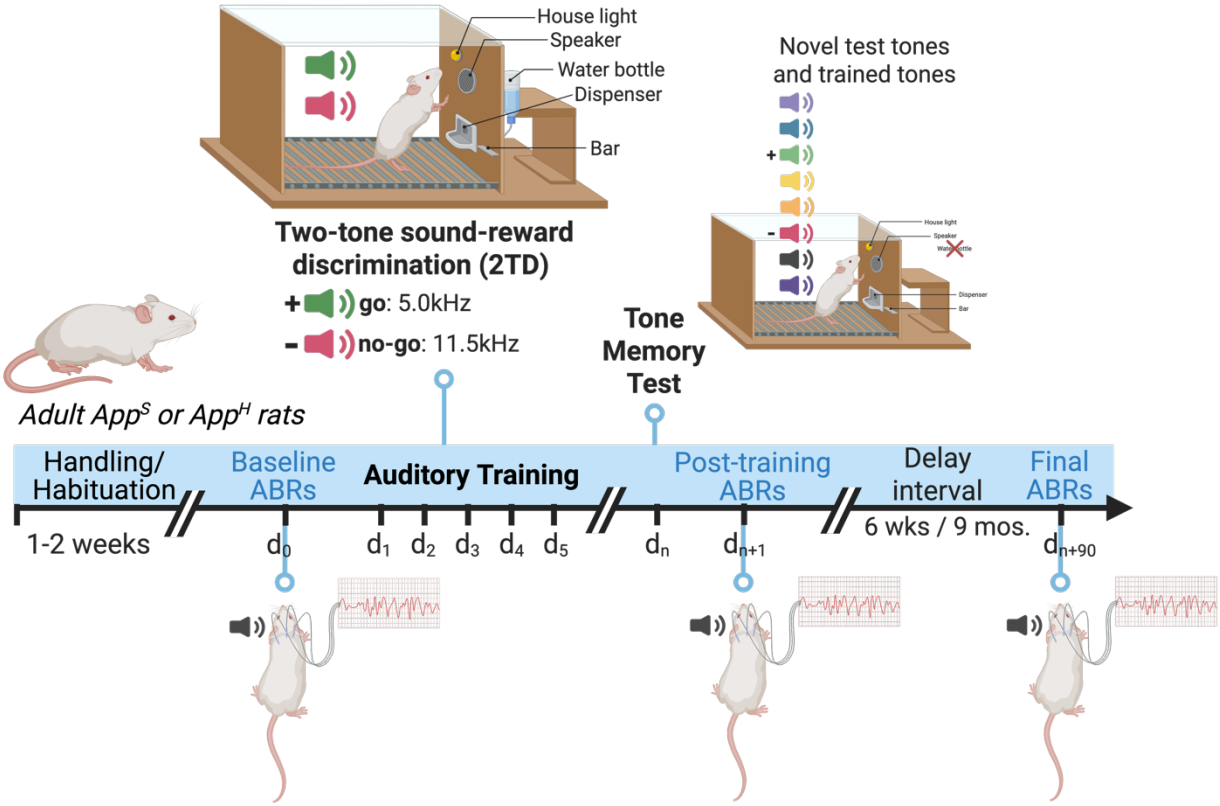

Supplemental Figure S4: *Experimental timeline*. Behavioral training was in an auditory cognitive task for sound-reward learning in parallel with electrophysiology in App^S and App^H rats. All rats were handled prior to the experimental procedures, then underwent sound-guided cognitive training in a two-tone discrimination task (2TD), followed by a memory test. The 2TD task requires rats to bar press to a rewarded "go" tone (5.0 kHz; 75 dB SPL) for a water reward, and to omit responding to an unrewarded "no-go" tone (11.5 kHz; 75 dB SPL) to avoid time-outs that extend the time to the next trial. A memory test occurred 24 hrs after the final training session and included eight pure tones of different frequencies (including the "go" and "no-go" frequencies). Bar press numbers were recorded and analyzed for each test tone separately to determine the success of auditory memory formation for the rewarded "go" tone after training. Tone-evoked ABRs were recorded in trained animals at three timepoints: prior to the first 2TD training session (baseline or pre-training), 24 hrs after the memory test (post-training), and after a delay (6 weeks later and 9 months later) to track training intervention-induced changes in auditory neurophysiological signals longitudinally.